

On spectral and temporal coherence of x-ray free-electron laser beams

Lutful Ahad,^{1,*} Ismo Vartiainen,¹ Tero Setälä,¹ Ari T. Friberg,¹
Christian David,² Mikako Makita,² and Jari Turunen¹

¹*Institute of Photonics, University of Eastern Finland, P. O. Box 111, FI-80101 Joensuu, Finland*

²*Paul Scherrer Institut, CH-5232 Villigen PSI, Switzerland*

*lutful.ahad@uef.fi

Abstract: A model for the coherence properties of free-electron lasers (FELs) in time and frequency domains is introduced within the framework of classical second-order coherence theory of nonstationary light. An iterative phase-retrieval algorithm is applied to construct an ensemble of field realizations in both domains, based on single-pulse spectra measured at the Linac Coherent Light Source (LCLS) in self-amplified spontaneous emission mode. Such an ensemble describes the specific FEL pulse train in a statistically averaged sense. Two-time and two-frequency correlation functions are constructed, demonstrating that the hard X-ray free-electron laser at LCLS in this case behaves as a quasistationary source with low spectral and temporal coherence. We also show that the Gaussian Schell model provides a good description of this FEL.

© 2016 Optical Society of America

OCIS codes: (030.1640) Coherence; (140.2600) Free-electron lasers (FELs); (340.7480) X-rays, soft x-rays, extreme ultraviolet (EUV).

References and links

1. C. Pellegrini and S. Reiche, "The development of X-ray free-electron lasers," *IEEE J. Sel. Top. Quantum Electron.* **10**, 1393–1404 (2004).
2. B. W. J. McNeil and N. R. Thompson, "X-ray free-electron lasers," *Nature Photon.* **4**, 814–821 (2010).
3. I. A. Vartanyats, A. Singer, A. P. Mancuso, O. M. Yefanov, A. Sakdinawat, Y. Liu, E. Bang, G. J. Williams, G. Cadenazzi, B. Abbey, H. Sinn, D. Attwood, K. A. Nugent, E. Weckert, T. Wang, D. Zhu, B. Wu, C. Graves, A. Scherz, J. J. Turner, W. F. Schlotter, M. Messerschmidt, J. Lüning, Y. Acremann, P. Heimann, D. C. Mancini, V. Joshi, J. Krzywinski, R. Soufli, M. Fernandez-Perea, S. Hau-Riege, A. G. Peele, Y. Feng, O. Krupin, S. Moeller and W. Wurth, "Coherence properties of individual femtosecond pulses of an x-ray free-electron laser," *Phys. Rev. Lett.* **107**, 144801 (2011).
4. J. P. Marangos, "Introduction to the new science with x-ray free-electron lasers," *Contemp. Phys.* **52**, 551–569 (2011).
5. J. Spence, "X-ray imaging: ultrafast diffract-and-destroy movies," *Nature Photon.* **2**, 390–391 (2008).
6. H. N. Chapman, P. Fromme, A. Barty, T. A. White, R. A. Kirian, A. Aquila, M. S. Hunter, J. Schulz, D. P. DePonte, U. Weierstall, R. B. Doak, F. R. N. C. Maia, A. V. Martin, I. Schlichting, L. Lomb, N. Coppola, R. L. Shoeman, S. W. Epp, R. Hartmann, D. Rolles, A. Rudenko, L. Foucar, N. Kimmel, G. Weidenspointner, P. Holl, M. Liang, M. Barthelmess, C. Caleman, S. Boutet, M. J. Bogan, J. Krzywinski, C. Bostedt, S. Bajt, L. Gumprecht, B. Rudek, B. Erk, C. Schmidt, A. Hömke, C. Reich, D. Pietschner, L. Strüder, G. Hauser, H. Gorke, J. Ullrich, S. Herrmann, G. Schaller, F. Schopper, H. Soltau, K-U. Kühnel, M. Messerschmidt, J. D. Bozek, S. P. Hau-Riege, M. Frank, C. Y. Hampton, R. G. Sierra, D. Starodub, G. J. Williams, J. Hajdu, N. Timneanu, M. M. Seibert, J. Andreasson, A. Rucker, O. Jönsson, M. Svenda, S. Stern, K. Nass, R. Andritschke, C-D. Schröter, F. Krasniqi, M. Bott, K. E. Schmidt, X. Wang, I. Grotjohann, J. M. Holton, T. R. M. Barends, R. Neutze, S. Marchesini, R.

- Fromme, S. Schorb, D. Rupp, M. Adolph, T. Gorkhover, I. Andersson, H. Hirsemann, G. Potdevin, H. Graafsma, B. Nilsson, and J. C. H. Spence, "Femtosecond x-ray protein nanocrystallography," *Nature* **470**, 73–77 (2011).
7. H. N. Chapman and K. A. Nugent, "Coherent lensless x-ray imaging," *Nature Photon.* **4**, 833–839 (2010).
 8. M. Tegze and G. Faigel, "X-ray holography with atomic resolution," *Nature* **380**, 49–51 (1996).
 9. G. Grübel and F. Zontone, "Correlation spectroscopy with coherent x-rays," *J. Alloys Comp.* **362**, 3–11 (2004).
 10. R. Mitzner, B. Siemer, M. Neeb, T. Noll, F. Siewert, S. Rolling, M. Rutkowski, A. A. Sorokin, M. Richter, P. Juranic, K. Tiedtke, J. Feldhaus, W. Eberhardt, and H. Zacharias, "Spatio-temporal coherence of free electron laser pulses in the soft x-ray regime," *Opt. Express* **16**, 19909–19919 (2008).
 11. A. Singer, F. Sorgenfrei, A. P. Mancuso, N. Gerasimova, O. M. Yefanov, J. Gulden, T. Gorniak, T. Senkbeil, A. Sakdinawat, Y. Liu, D. Attwood, S. Dziarzhytski, D. D. Mai, R. Treusch, E. Weckert, T. Salditt, A. Rosenhahn, W. Wurth, and I. A. Vartanyants, "Spatial and temporal coherence properties of single free-electron laser pulses," *Opt. Express* **20**, 17480–17495 (2012).
 12. C. Gutt, P. Wochner, B. Fischer, H. Conrad, M. Castro-Colin, S. L. F. Lehmkuhler, I. Steinke, M. Sprung, W. Roseker, D. Zhu, H. Lemke, S. Bogle, P. H. Fuoss, G. B. Stephenson, M. Cammarata, D. M. Fritz, A. Robert, and G. Grübel, "Single shot spatial and temporal coherence properties of the SLAC Linac Coherent Light Source in the hard x-ray regime," *Phys. Rev. Lett.* **108**, 024801 (2012).
 13. Y. H. Jiang, T. Pfeifer, A. Rudenko, O. Herrwerth, L. Foucar, M. Kurka, K. U. Kühnel, M. Lezius, M. F. Kling, X. Liu, K. Ueda, S. Düsterer, R. Treusch, C. D. Schröter, R. Moshhammer, and J. Ullrich, "Temporal coherence effects in multiple ionization of N₂ via XUV pump-probe autocorrelation," *Phys. Rev. A* **82**, 041403(R) (2010).
 14. T. Pfeifer, Y. Jiang, S. Düsterer, R. Moshhammer, and J. Ullrich, "Partial-coherence method to model experimental free-electron laser pulse statistics," *Opt. Lett.* **35**, 3441–3443 (2010).
 15. O. Bryngdahl and F. Wyrowski, "Digital holography—computer-generated holograms," in *Progress in Optics*, E. Wolf, ed. (North-Holland, 1990), vol. 28, pp. 1–86.
 16. R. Trebino, ed., *Frequency-Resolved Optical Gating: The Measurement of Ultrashort Laser Pulses* (Kluwer, 2002), Chap. 4.
 17. L. Sereda, M. Bertolotti, and A. Ferrari, "Coherence properties of nonstationary light wave fields," *J. Opt. Soc. Am. A* **15**, 695–705 (1998).
 18. L. Mandel and E. Wolf, *Optical Coherence and Quantum Optics* (Cambridge University, 1995).
 19. R. Dutta, J. Turunen, and A. T. Friberg, "Michelson's interferometer and the temporal coherence of pulse trains," *Opt. Lett.* **40**, 166–169 (2015).
 20. R. Dutta, A. T. Friberg, G. Genty, and J. Turunen, "Two-time coherence of pulse trains and the integrated degree of temporal coherence," *J. Opt. Soc. Am. A* **32**, 1631–1637 (2015).
 21. A. C. Schell, "A technique for the determination of the radiation pattern of a partially coherent aperture," *IEEE Trans. Antennas Propag.* **AP-15**, 187–188 (1967).
 22. G. Genty, M. Surakka, J. Turunen, and A. T. Friberg, "Second-order coherence of supercontinuum light," *Opt. Lett.* **35**, 3057–3059 (2010).
 23. G. Genty, M. Surakka, J. Turunen, and A. T. Friberg, "Complete characterization of supercontinuum coherence," *J. Opt. Soc. Am. B* **28**, 2301–2309 (2011).
 24. S. Düsterer, "Determination of temporal FEL pulse properties: challenging concepts and experiments," *Proc. SPIE* **8078**, 80780H (2011).
 25. J. A. Terschlüsen, M. Agäker, M. Svanqvist, S. Plogmaker, J. Nordgren, J. E. Rubensson, H. Siegbahn, and J. Söderström, "Measuring the temporal coherence of a high harmonic generation setup employing a Fourier transform spectrometer for the VUV/XUV," *Nucl. Instrum. Meth. Phys. A* **768**, 84–88 (2014).
 26. M. Makita, P. Karvinen, D. Zhu, P. N. Juranic, J. Grünert, S. Cartier, J. H. Jungmann-Smith, H. T. Lemke, A. Mozzanica, S. Nelson, L. Patthey, M. Sikorski, S. Song, Y. Feng, and C. David, "High-resolution single-shot spectral monitoring of hard x-ray free-electron laser radiation," *Optica* **2**, 912–916 (2015).
 27. A. M. Kondratenko and E. L. Saldin, "Generation of coherent radiation by a relativistic electron beam in an undulator," *Part. Acceler.* **10**, 207–216 (1980).
 28. P. Pääkkönen, J. Turunen, P. Vahimaa, A. T. Friberg, and F. Wyrowski, "Partially coherent Gaussian pulses," *Opt. Commun.* **204**, 53–58 (2002).
 29. J. Turunen, in *Laser Beam Propagation: Generation and Propagation of Customized Light*, A. Forbes, ed. (CRC Press, 2014), Chap. 10.

1. Introduction

Owing to their high brightness, ultrashort pulse duration, and high degree of transverse spatial coherence, X-ray free-electron lasers (XFELs) [1–3] enable novel research in material science, structural biology, and condensed matter physics [4]. Most of the experimental techniques utilize the coherent fraction of the radiation, including methods such as serial femtosecond crystallography (SFX) [5, 6], coherent X-ray diffraction imaging (CXDI) [7], X-ray holography [8],

and X-ray photon correlation spectroscopy (XPCS) [9]. Hence a thorough understanding of the coherence properties of XFELs [10–13] is of paramount importance.

In this paper we present a numerical method for generating ensembles of pulses representing beams such as those produced by XFELs. These mathematically constructed fields describe the statistical properties of the pulse train in an ensemble-averaged sense. Rather than assuming average spectral and temporal data as in [14], we employ actual measured spectra of individual pulses together with partial knowledge of their average time-domain intensity to construct the spectral phases and the temporal pulse realizations. The XFEL pulses, being rather incoherent in time but originating within similar stochastic conditions, are each represented by an ensemble of realizations. The train of pulses is subsequently statistically governed by a collection of such ensembles, one for each measured spectrum. For the field reconstruction, we apply a temporal-domain counterpart of the spatial iterative Fourier-transform algorithm (IFTA) [15]. The one-dimensional phase retrieval problem does not possess a unique solution [16], and in our case we only have at our disposal the average pulse length in the time domain. The solution would be non-unique even if, in addition to the spectrum, we had access to the individual temporal intensity of each measurement. In our statistical analysis we use this ambiguity to advantage to build ensembles of field realizations for the measured pulses. In the phase retrieval process the correct spectrum is obtained by using it as an explicit condition in the frequency domain. Due to lack of detailed information, the mean temporal intensity is constructed to be Gaussian with the known average pulse length. This is accomplished by employing in the time domain a Gaussian weighting function whose width is appropriately adjusted as the iteration proceeds. Each of the ensuing fields may be regarded as a physically admissible XFEL pulse realization with exact correspondence in the time and frequency domains. Moreover, the ensembles representing the pulses statistically match the experimentally measured spectral and temporal results, and the ensemble associated with the whole pulse train can thereby be expected to faithfully reproduce the statistics of the XFEL source. From the overall ensemble of spectral and temporal field realizations we then construct two-frequency and two-time correlation functions [17], which describe pulse trains of partial spectral and temporal coherence fully within the framework of the classical second-order coherence theory of nonstationary light.

In previous investigations [10–13], time-domain coherence of XFEL pulse trains has been considered using a temporal correlation function that depends only on time delay. Such an approach is adequate for stationary fields [18], whereas two-time correlation functions and time-resolved measurements are needed to completely characterize the temporal coherence properties of pulse trains [19, 20]. We illustrate our model using spectra of individual XFEL pulses measured at the Linac Coherent Light Source (LCLS), which turns out to behave as a quasistationary source despite the femtosecond-scale pulse duration. In addition, the coherence properties of the XFEL source are found to match extremely closely the predictions of the Gaussian Schell model [18, 21].

2. Correlation functions

We denote the frequency-domain and time-domain (scalar, complex) electric fields of the n th individual pulse in a pulse train by $E_n(\omega - \omega_0)$ and $E_n(t)$, respectively. The mean frequency [18] of the pulse train is given by $\omega_0 = \int_0^\infty \omega S^2(\omega) d\omega / \int_0^\infty S^2(\omega) d\omega$, where $S(\omega)$ is the average spectrum defined below. Introducing further $\Omega = \omega - \omega_0$, we may write the spectral field representation of an individual pulse in the form

$$E_n(\Omega) = \sqrt{S_n(\Omega)} \exp[i\phi_n(\Omega)], \quad (1)$$

where $S_n(\Omega) = |E_n(\Omega)|^2$ represents the spectral density of the pulse and $\phi_n(\Omega)$ is its spectral phase. In the envelope representation, the temporal field is

$$E_n(t) = A_n(t) \exp(-i\omega_0 t), \quad (2)$$

where

$$A_n(t) = \sqrt{I_n(t)} \exp[i\phi_n(t)] = \int_{-\infty}^{\infty} E_n(\Omega) \exp(-i\Omega t) d\Omega, \quad (3)$$

and $I_n(t) = |E_n(t)|^2 = |A_n(t)|^2$ is the temporal intensity profile of an individual pulse, $\phi_n(t)$ being the envelope phase.

By regarding the individual pulses (which generally are of different spectral and temporal form) as members of a statistical ensemble, we may introduce correlation functions in both spectral and temporal domains. In the second-order coherence theory of nonstationary light, the appropriate spectral correlation function is the two-frequency cross-spectral density function (CSD), defined as an ensemble average

$$W(\Omega_1, \Omega_2) = \langle E^*(\Omega_1)E(\Omega_2) \rangle = \frac{1}{N} \sum_{n=1}^N E_n^*(\Omega_1)E_n(\Omega_2), \quad (4)$$

where N is the number of pulses in the ensemble. We may also view the CSD as a function of the average and difference coordinates $\Omega = \frac{1}{2}(\Omega_1 + \Omega_2)$ and $\Delta\Omega = \Omega_2 - \Omega_1$. The mean spectrum of the pulse train is given by $S(\Omega) = W(\Omega, 0)$ and its complex degree of spectral coherence is defined as

$$\mu(\Omega, \Delta\Omega) = \frac{W(\Omega, \Delta\Omega)}{\sqrt{S(\Omega - \Delta\Omega/2)S(\Omega + \Delta\Omega/2)}}. \quad (5)$$

Considered as a function of $\Delta\Omega$, the characteristic breadth of $|\mu(\Omega, \Delta\Omega)|$ provides the spectral coherence width of the pulse train at frequency Ω .

Time-domain correlations of nonstationary fields are characterized by the two-time mutual coherence function (MCF), defined as

$$\Gamma(t_1, t_2) = \langle E^*(t_1)E(t_2) \rangle = \exp[-i\omega_0(t_2 - t_1)] \frac{1}{N} \sum_{n=1}^N A_n^*(t_1)A_n(t_2). \quad (6)$$

We may express the MCF in terms of the average and difference coordinates $t = \frac{1}{2}(t_1 + t_2)$ and $\Delta t = t_2 - t_1$. Then the mean temporal intensity is given by $I(t) = \Gamma(t, 0)$ and the complex degree of temporal coherence is defined as

$$\gamma(t, \Delta t) = \frac{\Gamma(t, \Delta t)}{\sqrt{I(t - \Delta t/2)I(t + \Delta t/2)}}. \quad (7)$$

Again, if we consider $|\gamma(t, \Delta t)|$ as a function of Δt , its width is a measure of the coherence time at time instant t . We emphasize that the spectral coherence width may depend strongly on Ω and the coherence time on t ; extreme variations occur, for instance, in supercontinuum pulse trains [22, 23].

Time-resolved measurements of the temporal (and spectral) intensity and phase of individual ultrashort pulses are possible in the visible region, which in principle allow a direct construction of the two-time and two-frequency correlation functions. Measurement of the temporal properties of XFEL pulses has been intensively studied [24]. However, to our knowledge there are no

methods that can provide the required temporal resolution or information about the temporal phase. Coherence measurements yielding time-integrated results in Michelson-type interferometric setups have been performed [25], but they do not enable the construction of the full two-time MCF. This raises the question what information can be extracted from such measurements.

It follows at once from Eqs. (2)–(4) and (6) that the CSD and MCF are related by the generalized Wiener–Khintchine theorem as

$$\Gamma(t_1, t_2) = \exp[-i\omega_0(t_2 - t_1)] \iint_{-\infty}^{\infty} W(\Omega_1, \Omega_2) \exp[i(\Omega_1 t_1 - \Omega_2 t_2)] d\Omega_1 d\Omega_2, \quad (8)$$

which, if the average and difference coordinates are used, becomes

$$\Gamma(t, \Delta t) = \exp(-i\omega_0 \Delta t) \iint_{-\infty}^{\infty} W(\Omega, \Delta\Omega) \exp[-i(\Omega \Delta t + \Delta\Omega t)] d\Omega d\Delta\Omega. \quad (9)$$

Inverting this expression, we find that the mean spectrum of the pulse train is given by

$$S(\Omega) = \frac{1}{(2\pi)^2} \iint_{-\infty}^{\infty} \Gamma(t, \Delta t) \exp[i(\omega_0 + \Omega)\Delta t] dt d\Delta t. \quad (10)$$

Since temporally integrated Michelson-type measurements provide us with the quantity

$$\bar{\Gamma}(\Delta t) = \frac{1}{2\pi} \int_{-\infty}^{\infty} \Gamma(t, \Delta t) dt, \quad (11)$$

the average spectrum may be written in the form

$$S(\bar{\omega} - \omega_0) = \frac{1}{2\pi} \int_{-\infty}^{\infty} \bar{\Gamma}(\Delta t) \exp(i\bar{\omega}\Delta t) d\Delta t, \quad (12)$$

where $\bar{\omega} = (\omega_1 + \omega_2)/2$. This result is formally equivalent with the classic Wiener–Khintchine theorem for stationary light [18]. However, instead of the MCF for stationary fields, we consider here the time integral of the two-time MCF. Equation (12) shows that the mean spectrum of a pulse train is obtained from time-integrated Michelson interferometer measurements. In reverse, the time-integrated MCF can be obtained from the mean spectrum according to

$$\bar{\Gamma}(\Delta t) = \int_0^{\infty} S(\bar{\omega} - \omega_0) \exp(-i\bar{\omega}\Delta t) d\bar{\omega}. \quad (13)$$

The characteristic width of the normalized form of the temporally integrated MCF,

$$\bar{\gamma}(\Delta t) = \bar{\Gamma}(\Delta t)/\bar{\Gamma}(0), \quad (14)$$

may then be considered as a measure of the effective coherence time of the pulse train.

3. Iterative Fourier-transform algorithm (IFTA)

Our model for constructing ensembles of pulses, illustrated in Fig. 1, is based on the knowledge of a large number of spectra of individual pulses that have been measured for XFEL source at LCLS using full pulse energy of ~ 2 mJ, repetition rate of 120 Hz, mean photon energy of ~ 8.37 keV, and pulse length of 34 fs (corresponding to a FWHM of 40 fs). More details of the experiment can be found in [26]. In the time domain we assume that the mean temporal evolution of the pulse train is of the Gaussian form

$$I(t) = I_0 \exp(-2t^2/T^2), \quad (15)$$

where the mean pulse duration is $T = 34$ fs. Nevertheless, shorter Gaussian pulses and also any non-Gaussian mean pulse shapes, which could arise in different FEL operation regimes, could be considered equally well by using an appropriate average pulse shape. Under such conditions the pulse train might exhibit different statistics, but the method presented here would still be fully applicable.

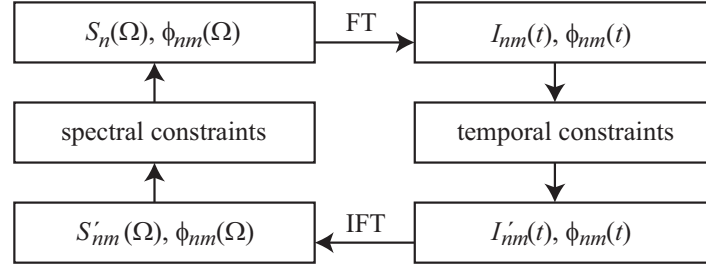


Fig. 1. Flow chart of the temporal iterative Fourier-transform algorithm (IFTA).

In the initialization stage of the algorithm we associate with the (measured) pulse spectrum $S_n(\Omega)$ of the n th field realization a random phase distribution $\phi_{n1}(\Omega)$ to generate the initial spectral field $E_{n1}(\Omega) = \sqrt{S_{n1}(\Omega)} \exp[i\phi_{n1}(\Omega)]$, as in [14]. We then use Eq. (3) to transform into the time domain, which gives $A_{n1}(t) = \sqrt{I_{n1}(t)} \exp[i\phi_{n1}(t)]$. The temporal constraints in Fig. 1 mean that the time-domain intensity distribution of the pulse is multiplied by a Gaussian function of the same form as in Eq. (15), but with the width given by $m \times 37$ fs, where m is the order of the iteration round in question. Starting from $T = 37$ fs and increasing the width at each iteration step (so that eventually the Gaussian is almost flat) was found to lead to the average intensity whose e^{-2} -width is 34 fs. The temporal phase of the field is left untouched implying that the time-domain field at this stage is $A'_{n1}(t) = \sqrt{I'_{n1}(t)} \exp[i\phi_{n1}(t)]$. We next make use of the inverse of Eq. (3), i.e.,

$$E'_{n1}(\Omega) = \frac{1}{2\pi} \int_{-\infty}^{\infty} A'_{n1}(t) \exp(i\Omega t) dt, \quad (16)$$

to convert back into the frequency domain. Here we set the spectrum to its measured form but leave the phase as it is, thus obtaining $E_{n2}(\Omega) = \sqrt{S_{n2}(\Omega)} \exp[i\phi_{n2}(\Omega)]$. The iterative process is continued as long as needed for the results to converge, i.e., until we achieve the situation $S'_{nm}(\Omega) = |E'_{nm}(\Omega)|^2 \approx S_n(\Omega)$.

4. Results and discussion

The algorithm results in an ensemble of pulse realizations with individual spectra that match the measured ones but have certain spectral phase distributions as well as temporal intensity profiles and phases that differ from one another. The CSD and MCF are then constructed using Eqs. (4) and (6). A single execution of the IFTA algorithm was found to lead to a temporal pulse of varying complicated shape, which depends on the chosen random initial spectral phase. This demonstrates a low degree of phase correlations for the individual XFEL pulses, defined as

$$\begin{aligned} \Phi(\Omega_1, \Omega_2) &= \langle \exp[-i\phi(\Omega_1)] \exp[i\phi(\Omega_2)] \rangle \\ &= \frac{1}{L} \sum_{l=1}^L \exp[-i\phi_l(\Omega_1)] \exp[i\phi_l(\Omega_2)] \end{aligned} \quad (17)$$

and

$$\begin{aligned}\Theta(t_1, t_2) &= \exp(-i\omega_0\Delta t) \langle \exp[-i\phi(t_1)] \exp[i\phi(t_2)] \rangle \\ &= \exp(-i\omega_0\Delta t) \frac{1}{L} \sum_{l=1}^L \exp[-i\phi_l(t_1)] \exp[i\phi_l(t_2)]\end{aligned}\quad (18)$$

in the spectral and temporal domains, respectively. The summation here is taken over L realizations obtained for an individual measured spectrum. To construct the CSD and MCF using Eqs. (4) and (6), we therefore average over a grand ensemble consisting of L realizations for each of the M single spectral pulse measurements in the pulse train. These final ensembles, both in time and frequency domains, thus contain a total of $N = M \times L$ realizations.

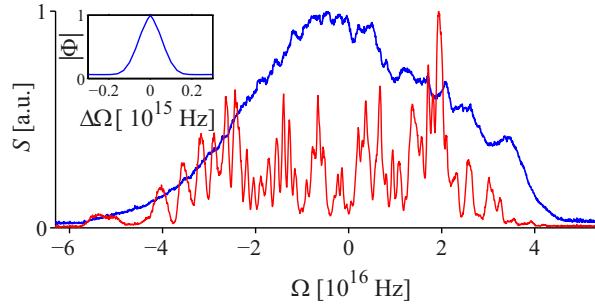


Fig. 2. Experimentally measured spectrum (solid red line) of a single pulse and the mean spectrum (solid blue line) of 1100 measured pulses. The mean spectrum equals the average spectrum calculated through IFTA. The inset shows the magnitude of the normalized average spectral phase-correlation function Φ constructed with 200 spectral field realizations related to the single-pulse spectrum.

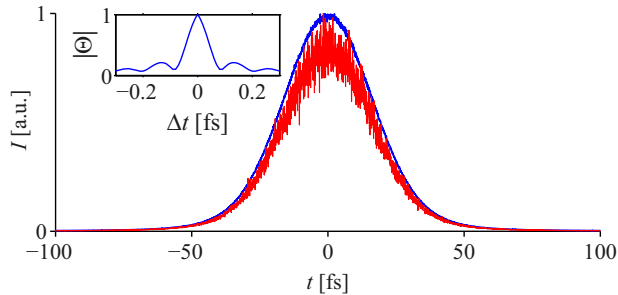


Fig. 3. Temporal intensity distribution (red line) constructed by averaging over 20 field realizations computed by IFTA with different phases associated with the single measured pulse shown in Fig. 2. The mean temporal intensity (blue line) is found by reconstructing with IFTA 20 realizations of varying phase profiles for each of the 1100 measured spectra, to obtain 22000 time-domain realizations, and averaging. The inset shows the magnitude of the normalized temporal phase-correlation function Θ calculated by averaging over 200 realizations with the same measured spectrum.

Numerical results, averaged over $M = 1100$ measured pulses with $L = 20$ realizations for each, are shown in Figs. 2 and 3. The spectral phase correlation function Φ of a single pulse,

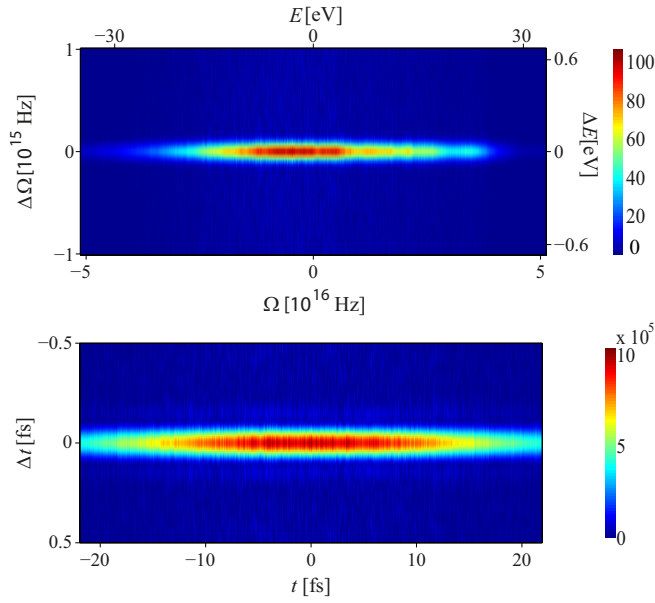


Fig. 4. Absolute values of the CSD (top, shown also in terms of the related photon energies E and ΔE) and the MCF (bottom) corresponding to 22000 reconstructed pulse realizations.

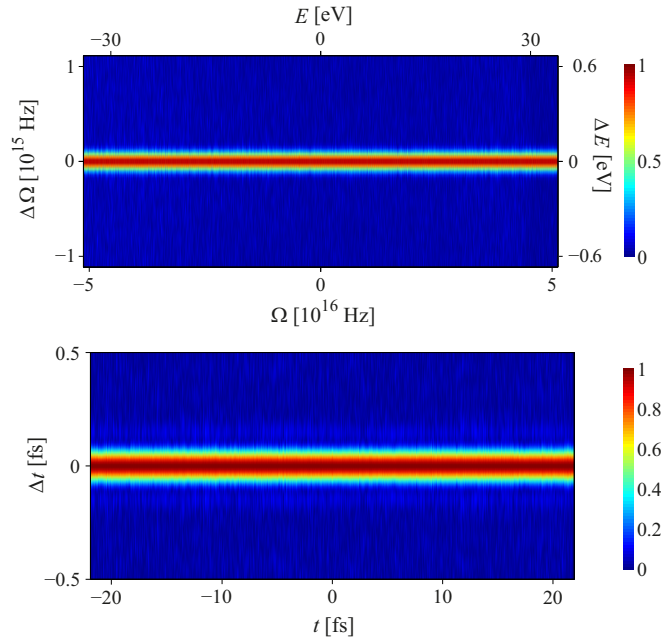


Fig. 5. Complex degrees of spectral (top) and temporal (bottom) coherence of the XFEL pulses. The top figure is shown also in terms of the associated photon energies E and ΔE .

displayed in the inset of Fig. 2, is constructed using Eq. (17) with $L = 200$ realizations (for better accuracy) and averaged over the frequencies. We see that its effective width in $\Delta\Omega$ is only a tiny fraction of the mean spectral spread of the pulses. The corresponding temporal intensity

distributions, together with the time-averaged phase correlation function given by Eq. (18), are illustrated in Fig. 3. Clearly, the effective width of Θ in Δt is a small fraction of the mean temporal pulse duration. Like most FELs operating today, this source is based on self-amplification of spontaneous emission (SASE) [27]. Spontaneous gain gives rise to variations from bunch to bunch leading to large shot-to-shot spectral diversity, as seen from Fig. 2, and indicating a low degree of spectral coherence. This fact is reflected in the CSD and MCF plots displayed in Fig. 4, which appear as narrow horizontal lines (note the different scales on the horizontal and vertical axes).

The normalized CSD and MCF, defined by Eqs. (5) and (7), respectively, are shown in Fig. 5. They confirm the low spectral and temporal coherence and the almost stationary nature of the XFEL pulse train. The width of $|\mu(\Omega, \Delta\Omega)|$ in the $\Delta\Omega$ direction (spectral coherence width) is nearly independent of Ω , i.e., $|\mu(\Omega, \Delta\Omega)| \approx |\mu(\Delta\Omega)|$, and similarly, the width of $|\gamma(t, \Delta t)|$ in the Δt direction (coherence time) is nearly independent of t , i.e., $|\gamma(t, \Delta t)| \approx |\gamma(\Delta t)|$. In this case, $|\gamma(\Delta t)|$ is essentially the integrated quantity $\bar{\gamma}(\Delta t)$ in Eq. (14). Figure 6 shows $|\mu(\Delta\Omega)|$ and $|\gamma(\Delta t)|$, averaged over Ω and t , respectively, together with Gaussian fits. Since the spectral coherence width is small compared to the average spectral spread and the coherence time is short compared to the mean pulse duration, this FEL behaves as a quasistationary source in the language of second-order coherence theory of nonstationary light.

We can approximate the XFEL pulse train using the Gaussian Schell model [18, 21, 28, 29]. The mean intensity then is given by the Gaussian function $I(t)$ of Eq. (15) (with duration T), the spectrum has a Gaussian form

$$S(\Omega) = S_0 \exp(-2\Omega^2/\Sigma^2), \quad (19)$$

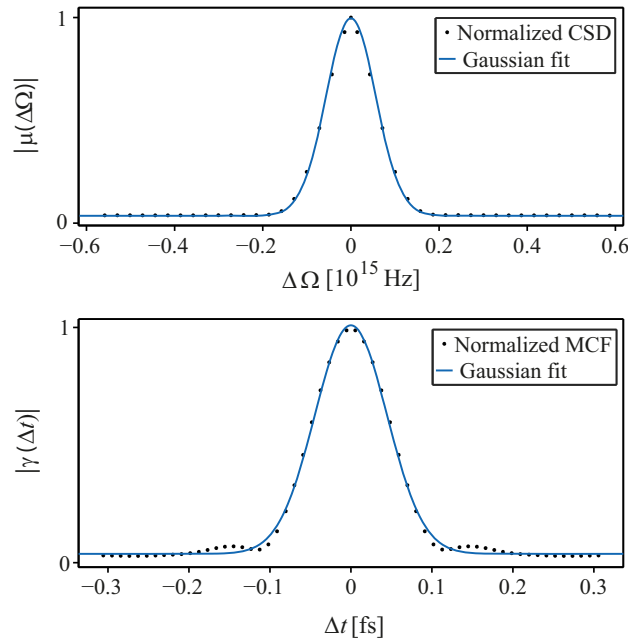


Fig. 6. Widths of the averaged normalized CSD (top) and the MCF (bottom) as functions of the difference coordinates. The dots represent the data points given by IFTA and the solid lines are Gaussian fits.

and we take Gaussian distributions for the complex degrees of spectral and temporal coherence,

$$\mu(\Omega, \Delta\Omega) = \exp(-\Delta\Omega^2/2\Sigma_\mu^2), \quad (20)$$

$$\gamma(t, \Delta t) = \exp(-\Delta t^2/2T_\gamma^2) \exp(-i\omega_0\Delta t), \quad (21)$$

respectively. The parameters T , Σ , Σ_μ , and T_γ are not independent. In the quasistationary case, when $\Sigma \gg \Sigma_\mu$, $T \gg T_\gamma$, and the time–bandwidth product $T\Sigma \gg 1$, the relations $\Sigma_\mu = 2/T$ and $T_\gamma = 2/\Sigma$ hold [29]. A Gaussian fit of the average spectrum shown in Fig. 2 gives $\Sigma = 4.35 \times 10^{16}$ Hz. Hence, with $T = 34$ fs, we have $T\Sigma = 1500$, $\Sigma_\mu = 5.9 \times 10^{13}$ Hz, and $T_\gamma = 0.046$ fs. Figure 6 displays the mean cross-sections $|\mu(\Delta\Omega)|$ and $|\gamma(\Delta t)|$ of the absolute values of the normalized CSD and MCF. The Gaussian fits give $\Sigma_\mu \approx 5.7 \times 10^{13}$ Hz and $T_\gamma \approx 0.046$ fs, in excellent agreement with the Gaussian Schell model. The widths of Gaussian functions in Fig. 6 correspond to a drop from the peak values of unity to $e^{-0.5}$ when the non-zero tails were taken into account.

5. Conclusions

We have introduced an iterative mathematical technique for the construction of ensembles of pulses in both spectral and temporal domains. The model is based on spectral measurements of individual pulses and on knowledge of the mean pulse duration. Such ensembles were used to construct two-time and two-frequency correlation functions that fully describe the second-order coherence properties of the pulse train. In an explicit example we considered a particular FEL, which turned out to emit quasistationary pulse trains (with low spectral and temporal coherence). In addition, the source was found to obey the Gaussian Schell model. We emphasize, however, that the method put forward here is applicable to any other FEL, some of which are likely to be far more coherent, and in fact to any other pulsed laser source.

Acknowledgments

This work was partially funded by the Academy of Finland (projects 268480 and 268705) and Dean’s special support for coherence research at the University of Eastern Finland, Joensuu (project 930350). We acknowledge Sven Reiche from Paul Scherrer Institut for his comments on the manuscript. We also thank Diling Zhu and Yiping Feng from the Linac Coherent Light Source, SLAC National Accelerator Laboratory for their contributions in the spectral measurements. Toni Saastamoinen is acknowledged for assistance with the IFTA algorithm.